Materials and Design 191 (2020) 108655

Contents lists available at ScienceDirect

Materials and Design

journal homepage: www.elsevier.com/locate/matdes

Continuous monitoring of an intentionally-manufactured crack using an automated welding and in-process inspection system

Yashar Javadi *, Ehsan Mohseni, Charles N. MacLeod, David Lines, Momchil Vasilev, Carmelo Mineo, Euan Foster, Stephen G. Pierce, Anthony Gachagan

Centre for Ultrasonic Engineering (CUE), Department of Electronic & Electrical Engineering, University of Strathclyde, Glasgow G1 1XQ, UK

HIGHLIGHTS

- Automated weld deposition coupled with the real-time robotic NDT is discussed.
- An intentionally embedded defect, a tungsten rod, is introduced for verification.
- A partially-filled groove sample is also manufactured and ultrasonically tested.
- The system is then used for continuous monitoring of a crack for 20 h.
- The crack was initiated 22 min after the weld and grew for 1.5 h.

GRAPHICAL ABSTRACT

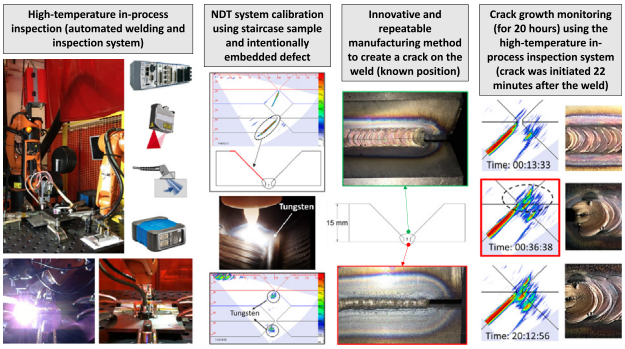

ARTICLE INFO

Article history:
Received 13 February 2020
Received in revised form 11 March 2020
Accepted 17 March 2020
Available online xxxx

Keywords:
Crack growth monitoring
Ultrasonic phased array
In-process inspection
Robotic NDE
Intentionally manufactured weld defects
Robotic welding

ABSTRACT

Automated weld deposition coupled with the real-time robotic Non-Destructive Evaluation (NDE) is used in this paper. For performance verification of the in-process inspection system, an intentionally embedded defect, a tungsten rod, is introduced into the multi-pass weld. A partially-filled groove (staircase) sample is also manufactured and ultrasonically tested to calibrate the real-time inspection implemented on all seven layers of the weld which are deposited progressively. The tungsten rod is successfully detected in the real-time NDE of the deposited position. The same robotic inspection system was then used to continuously monitor an intentionally-manufactured crack for 20 h. The crack was initiated 22 min after the weld ended and it grew quickly within the next 1.5 h. The crack growth stopped approximately after 2 h and no considerable change in the reflection signal was detected for the next 18 h of monitoring.

1. Introduction

1.1. In-process inspection

Traditionally, fusion welding and quality-control inspection of such welds are distinctly separate processes in the supply chain, which

* Corresponding author.
E-mail address: yashar.javadi@strath.ac.uk (Y. Javadi).

https://doi.org/10.1016/j.matdes.2020.108655

ultimately limit productivity, throughput and increase re-work. The opportunity exists to combine both of these practices directly at the point of manufacture through the use of new inspection, automation and control approaches. The concept of inspecting the welding process in real-time offers the possibility to control, adapt and consistently ensure high-quality defect-free welding. The use of modern automated welding strategies offers fundamental changes to the flexibility and range of possibilities, in terms of complexity and shape, of final fabrications. High-value thick complex welded components, typically feature multi-pass welds across multiple layers. Defects introduced in the lower layers which remain undetected until completion, result in the requirement for all remaining upper layers passes being mechanically removed to re-access the defecated lower layer [1]. Early detection of such defects would result in reduced re-work requirements and hence improved component build time and overall cost. Inspection of each pass during the welding process would allow the early and efficient screening of each layer and detection of any flaws. Even if the weld is not repairable, time and money will still be saved by early scrapping the component [1]. Such a concept has clear benefits to industrial organizations in both the quality of the final product and major improvements in production throughput. This has clear applicability to many industrial sectors that feature safety-critical multi-pass welds such as nuclear, energy (oil and gas, renewables) and defence [2–4]. Non-destructive evaluation (NDE) in the form of Ultrasonic Testing (UT) allows for such welds to be tested in a safe, efficient and unobtrusive manner. If the NDE is also implemented by a robotic system, fully-automated manufacturing and NDE can be a novel approach to a well-established manufacturing principle and has the potential to wholly reshape the approach, possibilities and direction of the global factories of the future.

The Phased Array Ultrasonic Testing (PAUT) method is used in this study for the in-process inspection which can be potentially performed by any non-contact NDT techniques such as Laser-Induced Ultrasonic Phased Array (LIPA) [5], thermography [6], eddy current [7], electromagnetic acoustic transducer (EMAT) [8], and X-ray/radiography [2]. However, due to the safety concerns surrounding radiography inspection [9], the lower penetration depth of eddy current (potentially a few millimetres [7]), less matured technology of LIPA [5], the lower resolution of thermography [7], and lower signal-to-noise ratio of EMAT [7,8] when compared with the phased array ultrasonic method [7], PAUT is preferred for this work.

1.2. Intentionally-manufactured weld defects

Welded specimens with intentionally embedded defects or flaws can be employed for training, development and research into procedures for NDE. They are more realistic and 3D representative of weld defects, for example, a tungsten rod can represent the lack of fusion more realistically than a side-drilled hole (SDH) manufactured later on the as-built sample [10,11]. Furthermore, the process of the intentional weld defect is mainly independent of the material machinability. This is beneficial for the materials which are hard to machine and then a suitable alternative for machining of small SDH. For verification of the in-process inspection system introduced in this study, it is critical to developing a repeatable manufacturing process to embed a defect in a controllable position of the weld. For example, since a number of uncertainties (can be potentially introduced during the robotic integration, high-temperature inspection, etc.) were involved in the first in-process inspection system developed for this work, a tungsten rod (a known size defect) intentionally embedded in a specific position of the weld was very beneficial to verify the system performance. In this study, two types of intentionally manufactured defects are used as follows:

I) Tungsten rod: In this study, the weld is deposited by the tungsten inert gas (TIG) welding method where the weld pool temperature never exceeds the melting temperature of the TIG electrode;

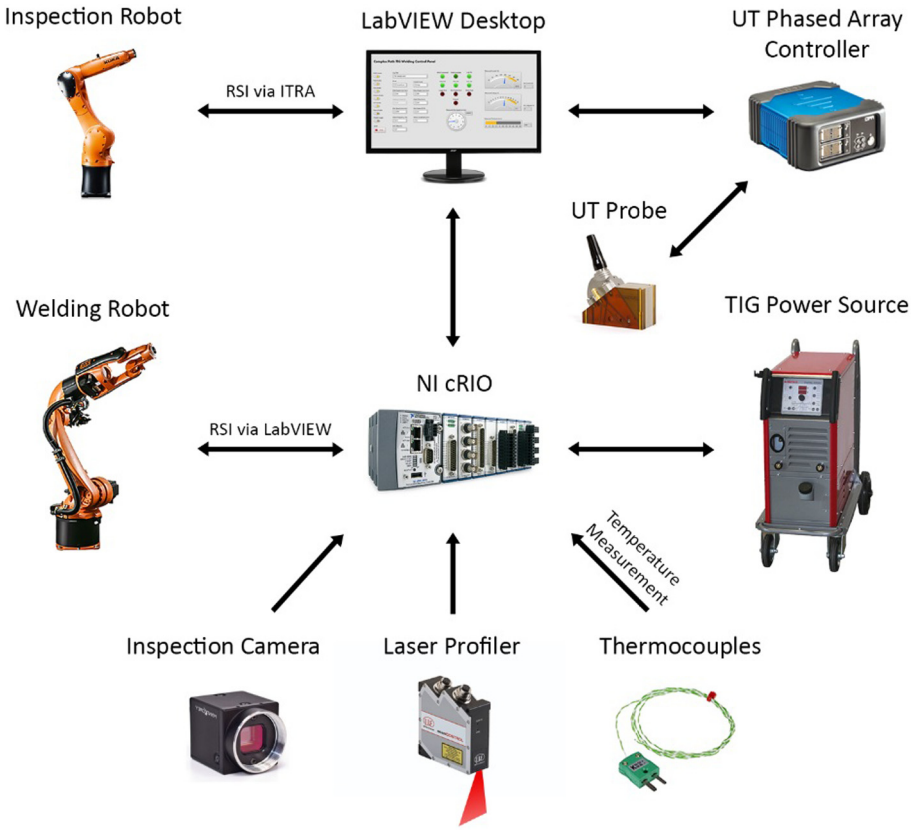

Fig. 1. The architecture of the robotic and integration system using cRIO, RSI and ITRA toolbox (the core of in-process robotic welding and inspection system).

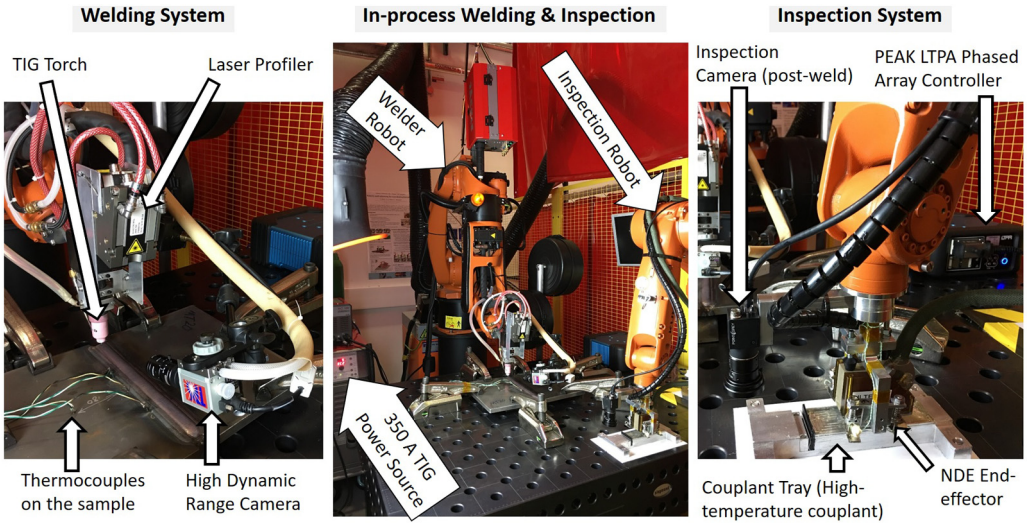

Fig. 2. Automated multi-pass welding and inspection system.

otherwise, the electrode will melt and the welding process terminated. Hence, the opportunity exists for the same TIG electrode to be used as an intentionally embedded defect inside a weld. The idea was first introduced by Javadi et al. [12] who showed that the tungsten carbide balls and tungsten rods can be embedded successfully inside the weld and they are good ultrasonic reflectors. Tungsten carbide balls were later used for calibration of a wire + arc additive manufacturing (WAAM) process too [13].

II) Crack: The in-process inspection system is expected to detect not only the cracks but also crack growth. Hence, a crack is intentionally manufactured in this study using a careful design of the experiment including a combination of welding parameters and material selection; i.e., (I) low current weld, (II) short length weld and (III) very high hardness feeding wire.

1.3. Crack growth monitoring

Initiation and growth of fatigue cracks can determine the remaining strength of materials and then the mechanisms of fatigue crack initiation have been studied since the beginning of the investigation of fatigue damage one hundred years ago [14]. Similarly, the measurement of fatigue crack growth rate is a well-documented topic thanks to the ASTM-E647 standard [15] and a number of books [16] and literature [17]. This has been also reflected in the application of NDE for the crack growth monitoring which is mainly on the fatigue cracks [14,18–20]. In this study, a crack is intentionally manufactured in the weld and its initiation and growth are both monitored by the ultrasonic phased array system. In comparison with the fatigue crack initiation methods which rely on the artificial machining of a notch or slot [15],

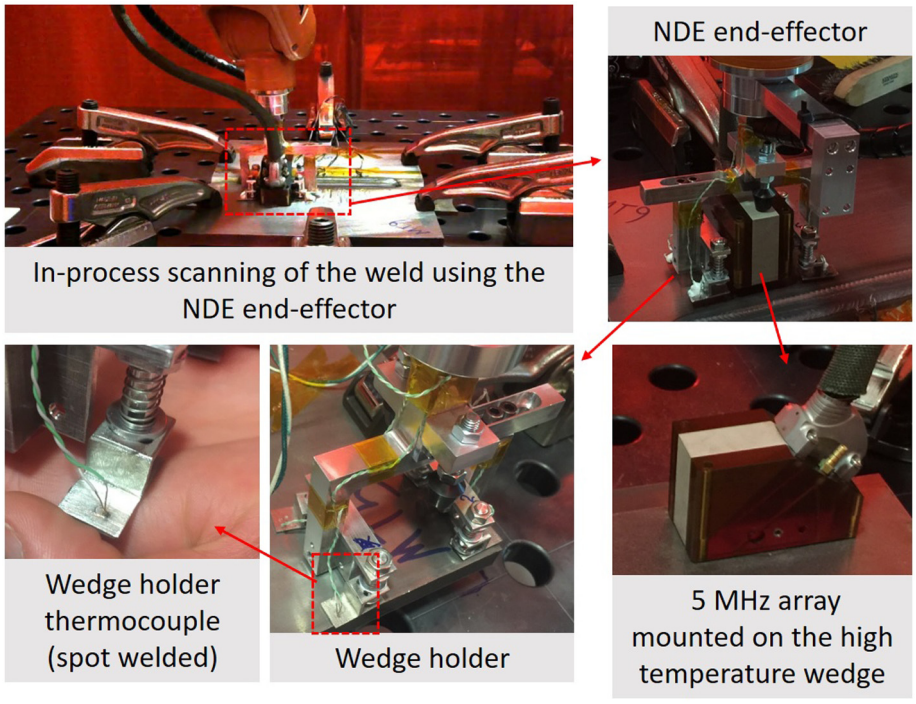

Fig. 3. In-process scanning of the weld using NDE end-effector.

there is no artificial or external crack trigger used in this paper. Alternatively, the welding parameters are changed to encourage crack initiation and growth. This innovative method of introducing the weld crack (a combination of welding parameters, groove design and the welding wire material) can result in the manufacturing of a more realistic defect in comparison with the fatigue crack.

2. The architecture of the robotic and integration system

The heart of in-process welding and inspection system used in this work is a sophisticated integration system including two robots, welding machine, phased array controller and a number of process monitoring devices which are all working simultaneously (see Fig. 1). For example, the welding machine (Tungsten Inert Gas, TIG, Power Source) is in charge of the welding arc (process parameters) but the welding torch is physically mounted on a robot (called welder robot here). This is the first step of the integration, i.e., the welder robot needs to communicate with the welding machine to correlate the welding path (robot positioning) with the welding parameters (the arc). This communication is controlled by a Compact Rio (cRIO), manufactured by the National Instrument (USA), and with a LabVIEW code. There is also some additional equipment (Laser Profiler, Inspection Camera and Thermocouple) required to be linked to this integration system as shown in Fig. 1. Furthermore, the inspection system (including the inspection robot, phased array controller and ultrasonic probe) is critical to be part of this integration architecture, otherwise,

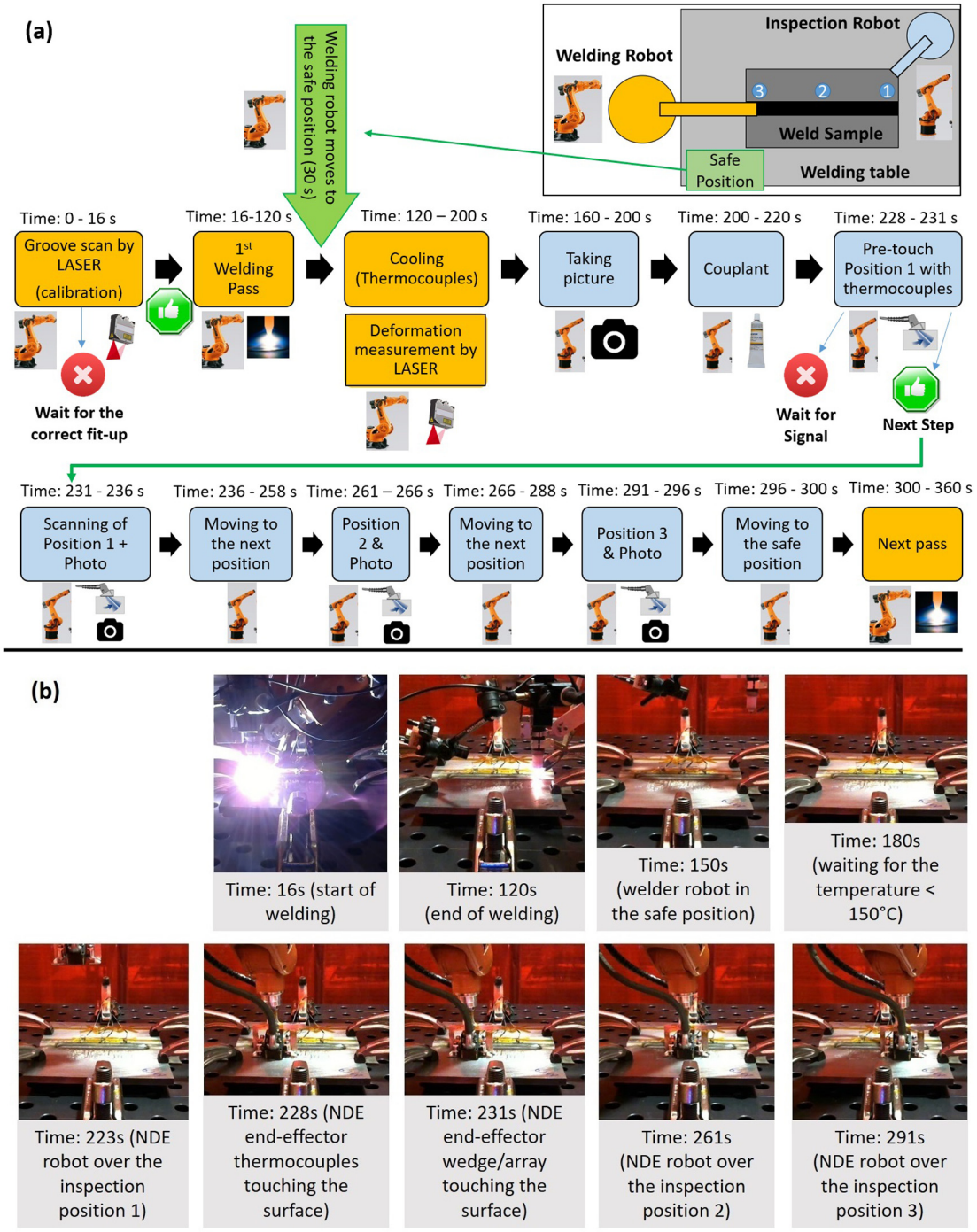

Fig. 4. In-process welding and inspection methodology (a: logical flowchart, b: experimental deployment).

Table 1
Welding parameters.

	Voltage (V)	Current (A)	Travel speed (mm/min)	Wire feed speed (mm/min)	Weaving amplitude (mm)	Weaving frequency (Hz)
Layer 1 (root pass)	AVC* set on 12 V	100–120**	50	910	2	0.3
Layer 2 (hot pass)	13.5	220	100	1225	4	0.6
Layer 3–6 (filling passes)	13.5	210	120	1470	3	0.55
Layer 7 (capping passes)	13.5	240	100	1225	4	0.6

Note 1: Gap was 2.55 mm at the start but 3.3 mm at the endpoint.
Note 2: Welding wire was ø1.2 mm (both normal and hard-facing wires were used in this work).
* Automatic Voltage Correction (AVC) using the RSI.
** To close the gap at the start, lower current (100 A) was used for 5–10 mm and then 120 A for the rest of 280 mm weld length.

the in-process inspection of the weld is impractical to achieve due to the interference of two main systems (e.g., a collision risk of the inspection robot with the welding robot). In order to construct a software interfacing layer between all components of the robotic welding system with in-process NDE capabilities, an in-house developed cross-platform software toolbox, named Interfacing Toolbox for Robotic Arms (ITRA), was used [21]. In this work, ITRA embedded functions were used through LabVIEW to interface some critical components of the system. This allowed controlling the sequence of the welding and data acquisition phases, by triggering the progress of the robot tool-paths and the collection of data through the thermocouples, the machine-vision cameras and the ultrasonic testing (UT) probe.

The industrial robots used in this study are both based on the 4th generation of KUKA Robot Controller (KRC4), equipped with a KUKA software add-on known as Robot Sensor Interface (RSI) as documented by KUKA [22]. RSI runs in a real-time manner to enable the communication between the robot controller and an external system (e.g. a sensor system or a server computer). For example, the automatic voltage correction (AVC) used in this work is not achievable without the RSI. Using the AVC, the welding robot is continuously correcting the Z position (welding stand-off) to keep the arc voltage consistent. Therefore, the RSI feature is implemented in the welding robot and is linked to the whole integration system through the LabVIEW as shown in Fig. 1. Similarly, the RSI is used in the inspection robot via ITRA and LabVIEW central code.

3. Experimental setup

3.1. In-process welding and inspection system

The automated multi-pass welding and inspection system used in this study is shown in Fig. 2. The Tungsten Inert Gas (TIG) welding process is deployed via a 6-axis KUKA robotic manipulator equipped with a TIG welding torch. The inspection process utilizes a separate 6-axis KUKA robot to deploy an NDE end-effector (Fig. 3) carrying a PAUT probe and angled wedge for shear wave inspection. The NDE end-effector has three main parts: (I) ultrasonic array, (II) high-temperature compliant wedge and (III) thermocouples. The ultrasonic array is a 5 MHz, 64 elements, 0.5 mm pitch array. The angled wedge (55°) is manufactured in an amorphous thermoplastic polyetherimide resin called ULTEM™ and is capable of withstanding intermittent temperatures as high as 150 °C. The wedge holder was also equipped with four spring-loaded thermocouples which first touch the specimen, before the wedge, in order to ensure the surface temperature is less than the wedge operational limit. High-temperature couplant is utilised between the wedge and the surface under inspection. A PEAK LTPA phased

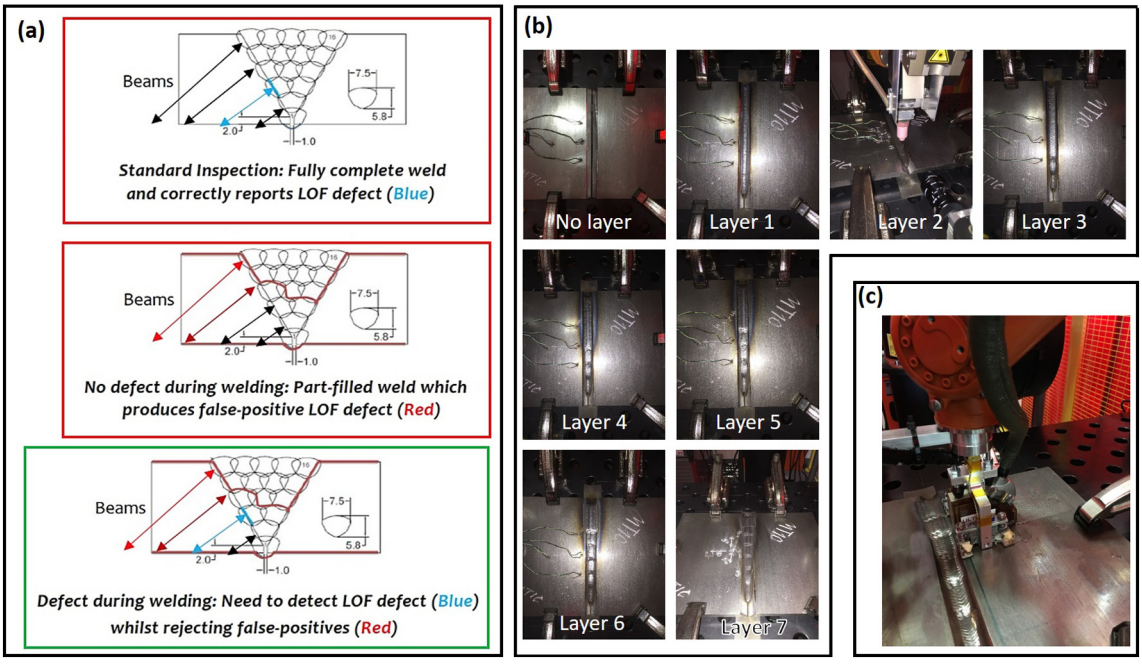

Fig. 5. Multi-pass weld beads layout.

Table 2
Manufacturing methods and samples investigated in this study.

Sample number	Description	Purpose
#1	Staircase (calibration) sample	Calibration of the inspection system concerning the ultrasonic wave reflection from the partially-filled weld groove
#2	Multi-pass welded sample with an intentionally-embedded tungsten	Verification of the in-process inspection system (high-temperature performance) using a known-size defect
#3	The weld sample with an intentionally-manufactured crack	Continuous monitoring of a crack for 20 h (verification of the in-process inspection system in a continuous working circumstance)

array controller was used for array control and signal acquisition with an active aperture of 64 elements. A National Instruments, Compact RIO 9038 real-time controller programmed in the LabView environment, is employed to control the TIG welding machine, welding robot, inspection robot, thermocouples and PAUT controller.

Using the LASER scanner, the weld groove is first scanned to calibrate the welder robot and ensuring the correct fit-up of the sample and, therefore, a smooth robot move in the centre of the groove (Fig. 4a). If the fit-up is acceptable, the robot positioning offsets are automatically implemented into the welding controller program (LabView) and then the autonomous deposition of the first welding pass is initiated. The LASER scanner and High Dynamic Range (HDR) cameras provide real-time process information and control to optimize deposition parameters. For the first welding pass with low travel speed (only 50 mm/min), the welding is completed within 120 s and then the welder robot moves to the safe position (see Fig. 4a) to avoid any possible collision with the inspection robot. The safe position, shown by a green box in Fig. 4a, is on the other side of the sample, opposite to the inspection side, to reduce the risk of collision between the welder robot and inspection robot. Permanent thermocouples attached to the specimen being welded monitor the surface temperature for overall process control purposes. After the completion of a single welding pass and the specimen surface temperature drops to 150 °C, the inspection robot initiates the NDE process (Fig. 4). Because the cooling takes time (e.g., around 100 s for the first pass shown in Fig. 4), this waiting time is used for taking pictures from the weld surface by the inspection camera mounted on the inspection robot. These pictures are all archived to be potentially used to correlate the internal defects with those visible imperfections captured during the real-time inspection. Furthermore, the waiting time is used to apply the high-temperature couplant underneath of the wedge by moving the NDE end-effector to the couplant tray.

The NDE end-effector is then deployed at multiple user-defined scanning positions along the welding axis (Fig. 4). The four thermocouples attached to the NDE end-effector first contact the sample surface and verify that the temperature is below the 150 °C limit. If so, the end-effector is deployed downward and the wedge and couplant make contact with the surface specimen. Three user-defined distinct inspection positions were selected along the weld axis each with a wedge contact duration of 5 s, deemed sufficient to achieve the desired ultrasonic data transmission and reception. The first position was 50 mm from the weld start, the second being in the centre of the weld length and the last was 50 mm distance to the weld endpoint.

The chosen array processing technique (FMC and/or Sectorial Scanning) is then generated and received data captured by the PA controller. The NDE process is repeated for each subsequent scanning position along the weld axis. Once all NDE scanning positions have been inspected, the inspection robot moves to the safe position to make the space clear for the welder robot to begin the next welding pass. The outlined procedure is repeated for all 21 welding passes required to complete the multi-pass weld.

3.2. Sample description

3.2.1. Process parameters and overview of the manufactured samples

The chosen specimens were 15 mm thick structural steel (S275) plates of length 300 mm. In total, 21 weld passes were deposited in 7 distinct layers inside a 90° degree V-groove. The welding parameters are listed in Table 1 and the weld layout is shown in Fig. 5.

Before the root pass, no tack-weld was deposited thanks to the implementation of varied gap method. Because the gap is gradually being closed with the weld moving forward in the root pass, a gap of 2.55 mm at the start of the weld but 3.3 mm at the endpoint was used. This has resulted in a consistent gap of 2.55 mm throughout the weld length. It is worth mentioning that the 3.3 mm was achieved following several trials aiming to develop the welding parameters which influence the gap design. Furthermore, closing the root gap at the start was practically difficult and then it was decided to start the weld with a lower current (100 A) and as soon as the gap was closed (usually after 5–10 mm and this could be simply confirmed by the weld camera), the current was reverted to the root pass current (120 A).

In this study, several trial and main samples were manufactured to calibrate and verify the in-process inspection system (see Table 2). However, the results of the main samples are only reported here and will be discussed in the following sections.

3.2.2. Partially-filled groove (staircase) sample (Sample #1)

For the in-process inspection of a multi-pass weld, it is required to manufacture and test a reference specimen containing all seven deposition layers in a partially-filled way (called staircase sample as shown in Fig. 6). The necessity of staircase sample is illustrated in Fig. 6a which shows how the in-process NDE results of a multi-pass welding process

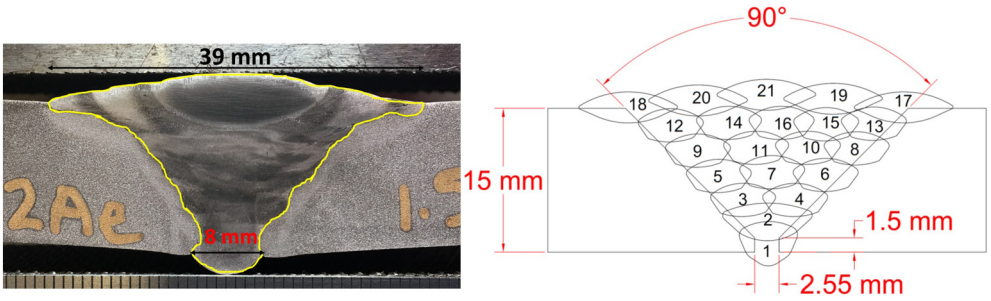

Fig. 6. The necessity (a), manufacturing (b) and robotic NDE (c) of staircase sample (Sample #1).

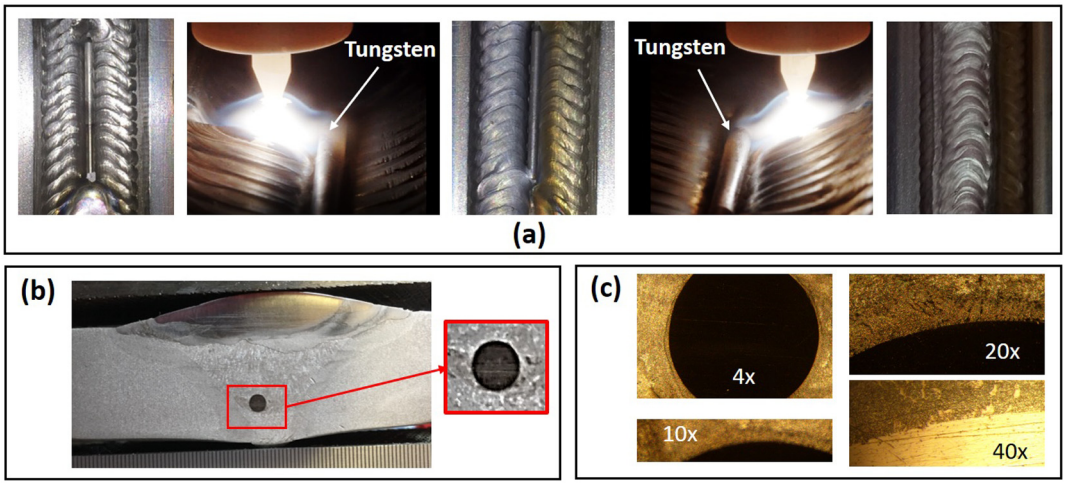

Fig. 7. Intentionally-embedded tungsten in a multi-pass welded sample, Sample #2 (a: manufacturing process, b: macrograph and c: microscopic investigations).

can be misinterpreted if the system has not previously calibrated by a staircase inspection experiment. The inspection whilst welding will require the amplitude threshold to be constrained to within a region of interest which progressively expands as the weld passes are laid down. The staircase test block, where the full range of weld cross-section profiles (containing all stages from none to fully welded as shown in Fig. 6b) is available in the same block, is, therefore, an ideal reference specimen. This sample is then tested with the same inspection robot (Fig. 6c) to provide consistent and reference configurations for the in-process inspection of the multi-pass welding.

3.2.3. The multi-pass welded sample with intentionally-embedded tungsten (Sample #2)

A real-time sector scan was implemented after each of 21 weld passes in three inspection positions, i.e., the first position is 50 mm from the weld start, the second being in the centre of the weld length and the last is 50 mm distance to the weld endpoint (see Fig. 4). Only in the second position, a ø2.6 mm tungsten rod of length 38 mm was intentionally embedded in the weld centre, within Pass 7 on layer 4 (see Fig. 7), to differentiate the centre NDE results from those obtained from the start and end positions. Therefore, if the in-process inspection system works properly, a visible difference has to be reflected in the sector scan image of the second position (with tungsten) in comparison with those captured in the first and third positions (without tungsten). Although there are various manufacturing methods for the intentional weld defects, all of them need to be verified themselves (as there is always possible that the defect is not manufactured properly) and then they cannot be used as verification of another system. The only exception is the tungsten embedding process because when the weld is monitored by the camera which shows the tungsten is covered by the subsequent weld layer, there is definitely an ultrasonic reflector permanently embedded in that position which can be used for verification of the in-process inspection system.

The manufacturing process included shortening of the Pass 7 length, i.e., stopping the arc 19 mm before the weld centre and restart it from 19 mm after the weld centre to produce an artificial slot with the length of 38 mm (same as the tungsten rod length as shown in Fig. 7a). Then, two passes on the left and right of the main pass can help to fix the tungsten rod in position with some tack-welds. The macrograph shows that the tungsten has not distorted or deformed (see Fig. 7b) and then a known shape defect has been successfully embedded in the weld. The microscopic investigations also prove that there is no air gap in the boundary of tungsten and the weld material (see Fig. 7c). This is an important manufacturing outcome required to avoid the complication of ultrasonic inspection of an unknown size/shape air gap/hole around the tungsten.

3.2.4. The weld sample with an intentionally-manufactured crack (Sample #3)

To manufacture a sample with crack, the following steps were required:

1) The weld needs to be very brittle to be prone to cracking. Therefore, a hard-facing wire (0.5% C, 3% Si, 0.5% Mn, 9.5% Cr and Fe: balance)

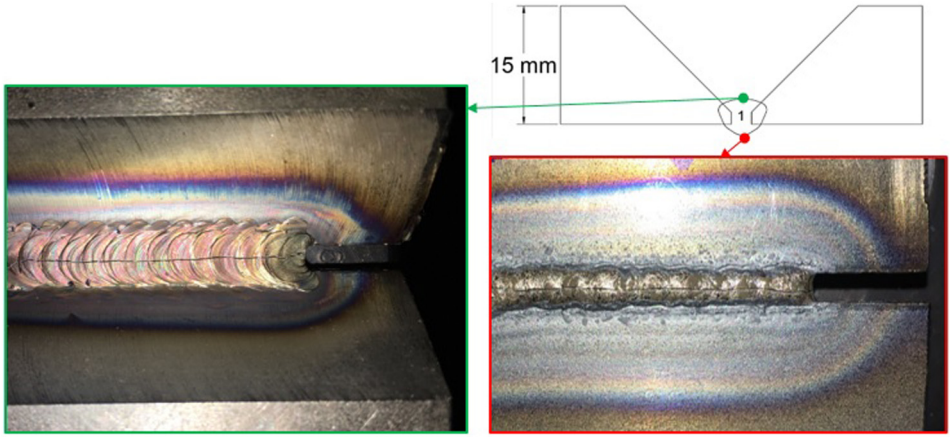

Fig. 8. Intentionally manufactured crack in weld (root pass); Sample #3.

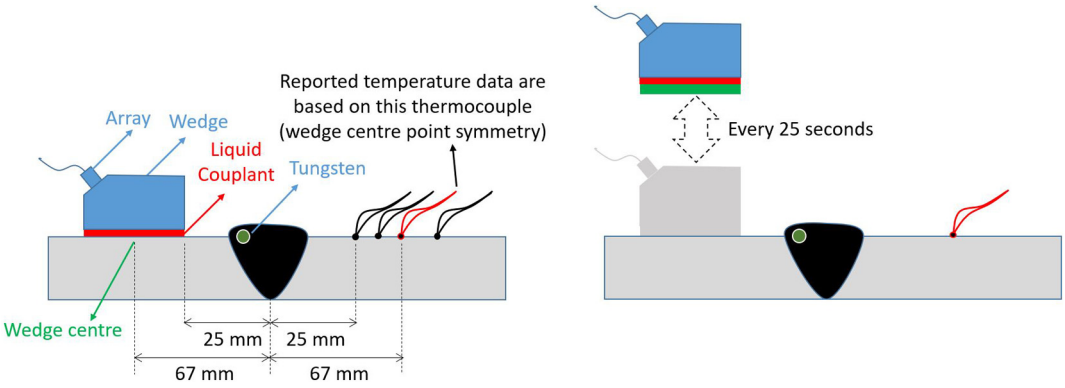

Fig. 9. The experimental setup to investigate the effect of temperature on the in-process inspection.

was used rather than the normal wire (0.08% C, 0.85% Si, 1.4% Mn, and Fe: balance) used in this study for the rest of samples. Based on the manufacturer reports, the first can achieve 50–60 HRC which is 2–3 times harder than the normal wire.

2) The weld must be very short (50 mm while the full weld length is normally 290 mm in this study) and just in one pass (root pass). This resulted in transferring all the clamping forces and residual stresses to a small brittle area [23,24].
3) Since the parent material is still a soft material (in comparison with the welding wire), the welding parameters are required to be chosen in a way to reduce the dilution (less participation of the parent material in the weld) in order to reach the maximum hardness in the weld. Hence, the welding current (normally 120 A for the root pass) was reduced to an amount just sufficient to melt the wire but not the parent material (i.e., 100 A). This method was tested on several samples and the weld monitoring camera could roughly show that the heat input was only sufficient to melt the wire and not the parent material. Hence, the participation of hard-facing wire in the root pass was maximum while the soft parent material part was minimum.

The combination of the above parameters has resulted in a large throughout crack from top to bottom of the weld and the length is almost the same as the weld length (see Fig. 8). Since this method was tested on several samples, it can be considered as a repeatable manufacturing process for the intentional weld crack.

3.3. Temperature effect on the in-process inspection

To investigate the effect of welding thermal gradient on the ultrasonic wave and in-process inspection, a temperature experiment was carried out with a setup shown in Fig. 9. The PAUT system was used to scan the main weld sample in a position allowing detection of intentionally-embedded tungsten (see Fig. 9). This scan was repeated every 25 s while the temperature was continuously being recorded by the thermocouples. This allowed the system to correlate the actual

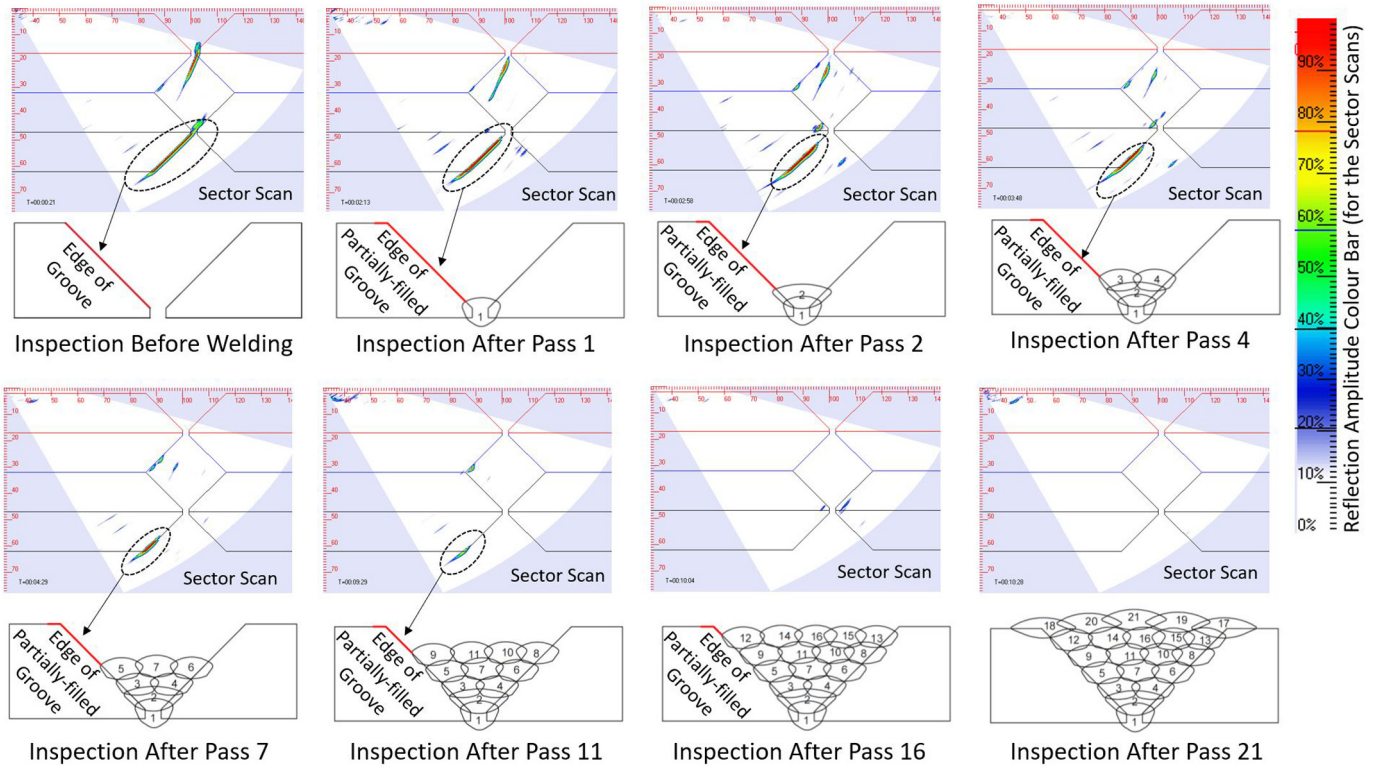

Fig. 10. Robotic NDE of the staircase sample (Sample #1).

reflection amplitude of each scan to the scanning temperature in a real weld sample (same thermal gradient expected in the in-process inspection).

4. Results and discussions

4.1. Calibration procedure (Sample #1)

The imaging approach selected was phased array sectorial scanning with a sweeping angle of 30–75° and step size of 0.5°. The horizontal distance (perpendicular axis to the weld length) between the wedge front face and the weld centre is 23 mm so that there is no direct contact between the weld cap and the wedge, instead, the wedge is always sitting over the parent material. The staircase sample (Sample #1) was tested in eight positions using the in-process inspection system developed in this study (see Fig. 10).

The reflection from the groove edge due to the partially filled weld is detected by the NDE system and then these signals will be removed from the subsequent in-process inspection of the multi-pass weld to increase the accuracy of the defect detection.

4.2. The effect of temperature on the in-process inspection

The results of temperature study are shown in Fig. 11. This proves that the ultrasonic inspection results can be considerably influenced by the temperature. For example, the defect position is 3 mm different between two inspections carried out at 28 °C and 164 °C. The reflection amplitude also changes from 62% to 25% with this temperature range. Since the in-process inspection is performed at a high temperature (150 °C in this work), it was necessary to know the temperature effect on the ultrasonic wave properties [25] and then this effect was measured and compensated for the in-process inspection.

4.3. Detection of tungsten using the in-process inspection (sample #2)

The imaging approach phased array configuration and horizontal distance between the wedge front face and the weld centre are all consistent with the staircase sample (Sample #1) inspection. The only differences are the sweeping angle (40–75° rather than the sweeping angle of 30–75°) and the gain. The first change is just for better illustration and has no effect on the results. The gain was 50 dB for the staircase

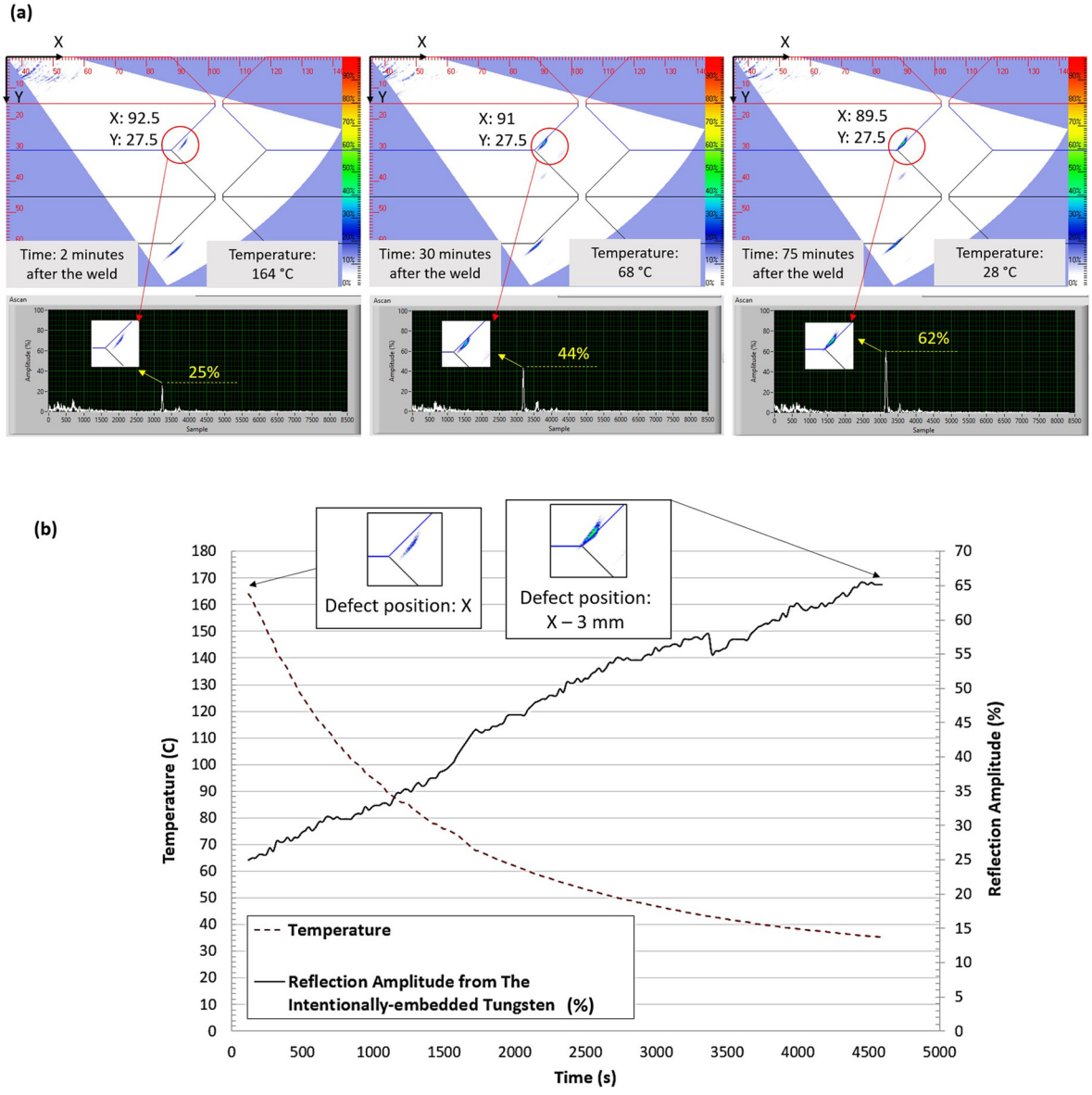

Fig. 11. The effect of temperature on the ultrasonic inspection of intentionally-embedded tungsten (a: three frames at the start, middle and end of the experiment – b: the whole experiment graph).

sample but it was increased to 60 dB in order to ensure that small defects (cracks) are detected by the system. Immediately after the deposition of the last pass, the tungsten rod was successfully detected in the deposited position while no lack of fusion defects at the start and end position were detected (Fig. 12). There is a good agreement between the detected position of tungsten rod with the NDE and the destructive macrograph results. The macrographs of start and endpoint also show defect-free sections which have already reported by in the NDE results (Fig. 12).

4.4. Crack growth monitoring (Sample #3)

The short root pass deposited in the Inspection Position 1, groove edge and not-filled groove (Inspection Positions 2 & 3) is detected with the in-process inspection system described in this study (see Fig. 13). These are the first images captured immediately after the welding, as soon as the temperature dropped <150 °C. The gain was consistent with the tungsten detection experiment, i.e., 60 dB as described in Section 4.1.

The inspection was continued for over 20 h and the results are shown in Fig. 14. The phased array sector scans are compared with the photographs taken by the camera mounted on the inspection robot. It is shown that there is no crack until 13 min after the weld end while very first signs of cracks can be seen 22 min (Time: 00:22:18 as highlighted in Fig. 14) after the weld. After a fast growth rate, the crack finished the main formation stage by 36 min after the weld (Time: 00:36:38) but it continued to grow within the next 1.5 h (until Time: 02:11:52). This crack was influenced by the material stress and then it was expected if it initiates, it would grow quickly. This is confirmed by the phased array inspection as there is no considerable increase in the reflection amplitude received from the crack between 2 and 20 h after the weld. Hence, the inspection was stopped after 20 h and once the sample was unclamped, it was found that the crack had been grown similarly in the root cap too (see bottom side observation in Fig. 14).

It is important to know whether the aforementioned figures (22 min, 36 min, etc.) will be consistent in repeat experiments. A key point is that the tungsten, which was detected successfully (Section 4.3), can be considered as the main verification for the high-temperature capability of the in-process inspection system developed in this study. Furthermore, the smooth and continuous trend of temperature effect on the reflection amplitude (Fig. 11) is a good indication of the repeatability of the robotic performance of the in-process inspection system. It is also not critical that this specific type of crack is initiated repeatably after 22 min. Instead, it is important that as soon as the crack is initiated, it can be successfully detected by the PAUT system. This was also verified by the inspection camera (since the crack was visible from the top surface) whose photographs matched the PAUT results (initiation and growth of the crack were both captured by the camera).

5. Conclusions

A combination of robotic multi-pass welding and automated phased array inspection is successfully implemented in this work. For verification purposes, a tungsten rod was intentionally embedded in the weld centre to differentiate the centre NDE results from those obtained from the start and end positions. Manufacturing and NDE of a staircase sample were also implemented for calibration of partially-filled weld groove required which is critical in the in-process inspection of the multi-pass welding process. This in-process welding and inspection system is then used to monitor an intentionally-manufactured crack. Based on the achieved results, it can be concluded that:

1) The macrograph and microscopic investigations proved that the tungsten rod was successfully embedded in the weld without any considerable change in the shape or size of the tungsten. There is also no unfused gap/hole in the boundary of tungsten and the weld material. Therefore, this method can be reliably used for validation of the in-process inspection because no unknown defect is produced along with the known size/shape tungsten rod.
2) Based on the real-time sector scanning results, an embedded tungsten rod was successfully detected in the deposited position while also showing no lack of fusion defects at the start and end position. This proves that the in-process inspection system developed in this study is accurate enough to differentiate the defect-less and defected sections in a high-temperature and real-time scanning configuration.
3) The staircase reference sample was successfully scanned using the in-process robotic inspection developed in this work. The data captured from the scanning of all seven partially-deposited layers

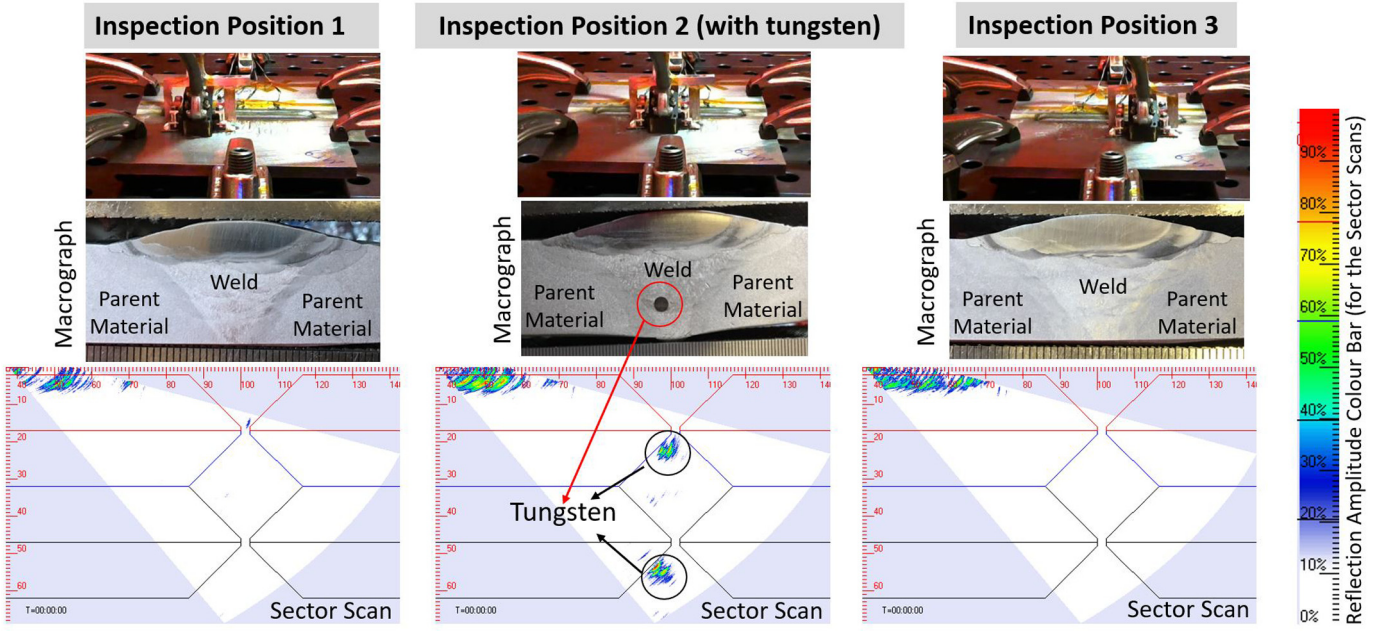

Fig. 12. Detection of tungsten rod using the in-process inspection of the multi-pass weld (Sample #2).

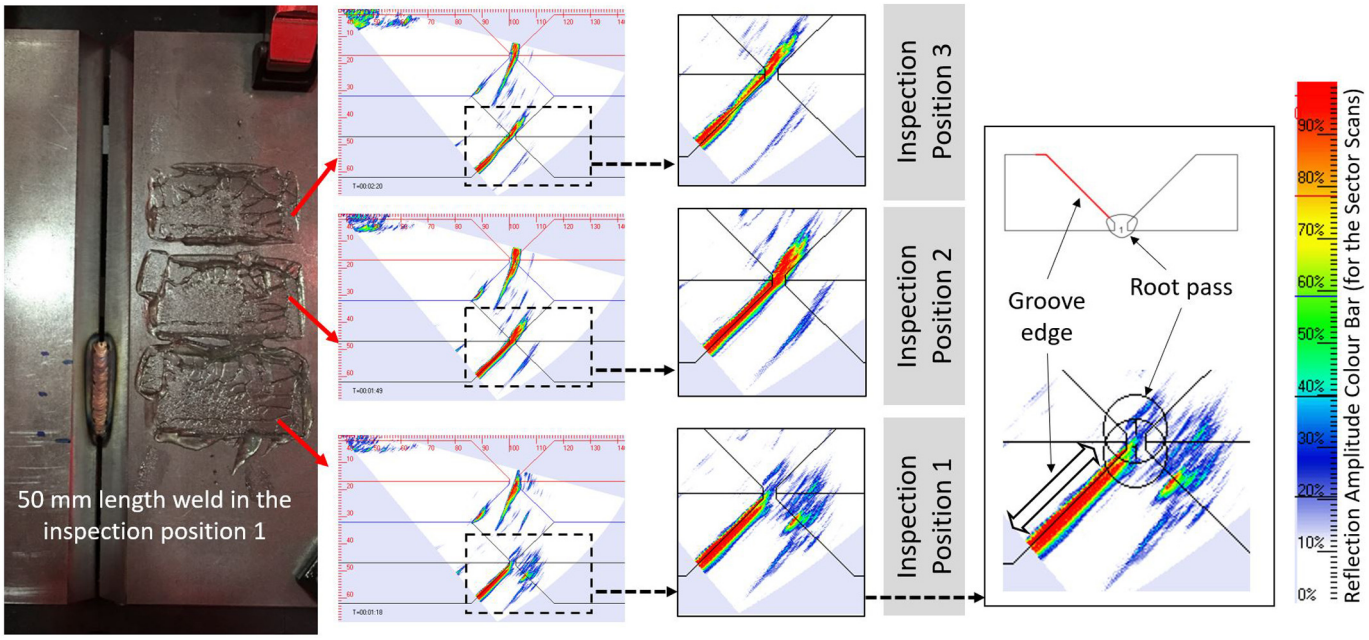

Fig. 13. In-process inspection of a short root pass (Sample #3).

were subsequently used for calibration of the in-process inspection system. The system detected the reflection from the partially filled groove during the inspection of the filling passes which vanishes once the cap passes are deposited. This step was critical before using the system for crack detection because the reflection signals received from crack and groove edge are required to be differentiated.

4) A crack was intentionally manufactured in the weld using a combination of low welding current, short root pass and hard-facing wire. This innovative method was tested on a few samples and then it can be introduced as a repeatable manufacturing process of the intentional weld crack.
5) Both the initiation and growth of the crack were successfully detected by the in-process inspection developed in this study during a 20-h continuous monitoring process.
6) The crack was initiated 22 min after the weld end, grew quickly in 15 min, continued growth within the next 1.5 h and then was stopped growing as the inspection results were identical between 2 and 20 h after the weld.

It is recommended to develop the in-process inspection for monitoring of known size defects in each pass of the multi-pass welds. Based on the results of this study, the root pass needed to be monitored for at least 36 min to where the crack grew considerably. In case of a fully

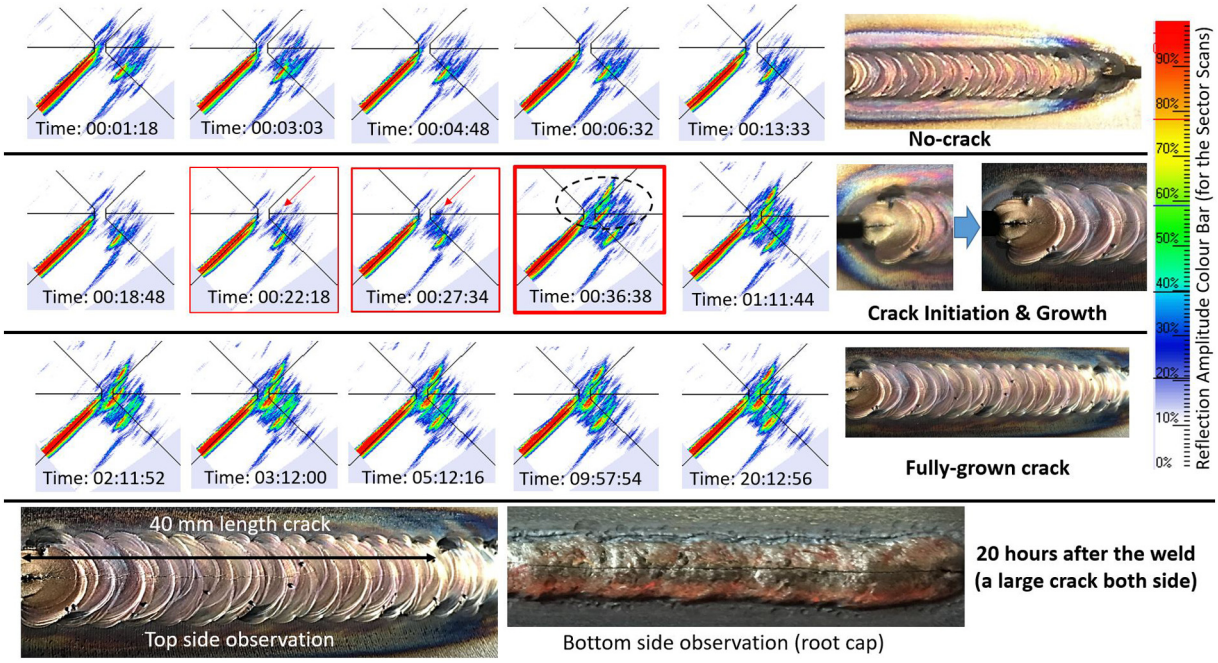

Fig. 14. Detection of crack initiation and growth using the in-process phased array inspection of the weld (Sample #3).

automated chain of manufacturing and inspection (Industry 4.0), it would be beneficial to monitor the root pass for a minimum of 36 min and if no crack is detected, the automatic pre-heating is required to be applied again and then the subsequent pass can be deposited. It is worth mentioning that the 36 min is just for the root pass deposited with the welding parameters developed in this study and then each sample requires to be first testified to find the proper in-process inspection delay time for every welding passes. Once these data are captured, the fully automated welding and inspection will be achieved and (I) automated multi-pass welding, (II) automated in-process inspection, (III) automated pre-heating, (IV) data processing and (V) intentionally-embedded defects for calibration along with integration of all of these systems are distinguished as the key requirements based on the concepts discussed in this study.

Declaration of competing interests

The authors declare that they have no known competing financial interests or personal relationships that could have appeared to influence the work reported in this paper.

CRediT authorship contribution statement

Yashar Javadi: Writing - original draft, Writing - review & editing, Investigation, Conceptualization, Methodology, Formal analysis.**Ehsan Mohseni:**Investigation, Formal analysis, Conceptualization.**Charles N. MacLeod:**Resources, Writing - original draft, Writing - review & editing, Conceptualization.**David Lines:**Investigation, Conceptualization, Writing - review & editing.**Momchil Vasilev:**Investigation, Conceptualization.**Carmelo Mineo:**Investigation, Conceptualization.**Euan Foster:** Investigation, Conceptualization.**Stephen G. Pierce:**Resources, Writing - original draft, Writing - review & editing, Conceptualization.**Anthony Gachagan:**Resources, Conceptualization, Writing - review & editing.

Acknowledgements

This work was undertaken as part of the UK Research Centre in NDE (RCNDE – EP/L022125/1) core project ABC of ARC. Furthermore, the concept of in-process inspection will be used in the Wire + Arc Additive Manufacturing (WAAM) projects which are all supported by EPSRC and InnovateUK as follows: (I) NEWAM (EP/R027218/1), (II) AIMaReM (EP/N018427/11) and (III) RoboWAAM (EP/P030165/1). The authors then like to acknowledge EPSRC, InnovateUK and RCNDE for the support and funding of the projects. The authors also like to acknowledge Mr. Grant Smillie for macrographs, Mr. George Cochrane and Mr. Alex Ward for machining.

Data availability

The data that support the findings of this study are available from the corresponding author on reasonable request.

References

[1] R.A. Smith, Non-Destructive Testing (NDT) – Guidance Document: An Introduction to NDT Common Methods, BINDT, 2015.
[2] Y. Sun, P. Bai, H.Y. Sun, P. Zhou, Real-time automatic detection of weld defects in steel pipe, NDT&E Int. 38 (2005) 522–528.
[3] Y.R. Zou, D. Du, B.H. Chang, L.H. Ji, J.L. Pan, Automatic weld defect detection method based on Kalman filtering for real-time radiographic inspection of spiral pipe, NDT&E Int. 72 (2015) 1–9.
[4] G. Wang, T.W. Liao, Automatic identification of different types of welding defects in radiographic images, NDT&E Int. 35 (2002) 519–528.
[5] T. Stratoudaki, Y. Javadi, W. Kerr, P.D. Wilcox, D. Pieris, M. Clark, Laser induced phased arrays for remote ultrasonic imaging of additive manufactured components, 57th the British Institute of Non-Destructive Testing Annual Conference, The British Institute of Non-destructive Testing (BINDT), Nottingham, United Kingdom 2018, p. 10.
[6] M. Vasudevan, N. Chandrasekhar, V. Maduraimuthu, A.K. Bhaduri, B. Raj, Real-time monitoring of weld pool during GTAW using infra-red thermography and analysis of infra-red thermal images, Weld. World 55 (2011) 83–89.
[7] P.J. Shull, Nondestructive Evaluation: Theory, Techniques, and Applications, CRC Press, 2002.
[8] W.M. Latham, D.T. MacLauchlan, D.P. Geier, D.D. Lang, EMAT Weld Inspection and Weld Machine Diagnostic System for Continuous Coil Processing Lines, SPIE, 1996.
[9] P. Cawley, Non-destructive testing — current capabilities and future directions, Proc. Inst. Mech. Eng. Pt. L-J. Mater.-Design Appl. 215 (2001) 213–223.
[10] Y. Javadi, M. Vasilev, C.N. MacLeod, S.G. Pierce, R. Su, C. Mineo, J. Dziewierz, A. Gachagan, Intentional weld defect process: from manufacturing by robotic welding machine to inspection using TFM phased array, 45th Annual Review of Progress in Quantitative Nondestructive Evaluation, AIP, Burlington, United States, 2018.
[11] M. Consonni, C.F. Wee, C. Schneider, Manufacturing of welded joints with realistic defects, Insight 54 (2012) 76.
[12] Y. Javadi, M. Vasilev, C.N. MacLeod, S.G. Pierce, R. Su, C. Mineo, J. Dziewierz, A. Gachagan, Intentional weld defect process: from manufacturing by robotic welding machine to inspection using TFM phased array, AIP Conference Proceedings 2102 (2019) 40011.
[13] Y. Javadi, C.N. MacLeod, S.G. Pierce, A. Gachagan, D. Lines, C. Mineo, J. Ding, S. Williams, M. Vasilev, E. Mohseni, R. Su, Ultrasonic phased array inspection of a wire + arc additive manufactured (WAAM) sample with intentionally embedded defects, Addit. Manuf. 29 (2019), 100806.
[14] L. Kunz, S. Fintová, Initiation of fatigue cracks in ultrafine-grained materials in high-cycle fatigue region, Procedia Eng. 74 (2014) 2–5.
[15] ASTM, Standard Test Method for Measurement of Fatigue Crack Growth Rates, E647 - 15e1, ASTM, 2016.
[16] Small-Crack Test Methods. , ASTM International, West Conshohocken, PA, 1992.
[17] M.H. Swain, Monitoring Small-Crack Growth by the Replication Method, ASTM International, West Conshohocken, PA, 1992.
[18] M. Corbetta, C. Sbarufatti, A. Manes, M. Giglio, Continuous crack growth monitoring and residual life prediction under variable-amplitude loading conditions, Procedia Eng. 74 (2014) 343–346.
[19] K.J. Kirk, A. McNab, A. Cochran, I. Hall, G. Hayward, Ultrasonic arrays for monitoring cracks in an industrial plant at high temperatures, IEEE Trans. Ultrason. Ferroelectr. Freq. Control 46 (1999) 311–319.
[20] E. Kostson, P. Fromme, Fatigue crack growth monitoring in multi-layered structures using guided ultrasonic waves, J. Phys. Conf. Ser. 195 (2009) 12003.
[21] C. Mineo, M. Vasilev, C.N. MacLeod, R. Su, S.G. Pierce, Enabling robotic adaptive behaviour capabilities for new industry 4.0 automated quality inspection paradigms, 57th Annual British Conference on Non-Destructive Testing, pp. 1–12.
[22] KUKA (Ed.), KUKA RobotSensorInterface (RSI) 3.2 Documentation, KUKA, 2013 , Version: KST RSI 3.2 V1.
[23] Y. Javadi, M. Akhlaghi, M.A. Najafabadi, Using finite element and ultrasonic method to evaluate welding longitudinal residual stress through the thickness in austenitic stainless steel plates, Mater. Des. 45 (2013) 628–642.
[24] Y. Javadi, M. Ashoori, Sub-surface stress measurement of cross welds in a dissimilar welded pressure vessel, Mater. Des. 85 (2015) 82–90.
[25] F.A. Silber, C. Ganglbauer, Ultrasonic testing of hot welds, Non-Destructive Testing 3 (1970) 429.